Anisotropic superconducting properties of single-crystalline $FeSe_{0.5}Te_{0.5}$

M. Bendele,[1,2,*] S. Weyeneth,[1] R. Puzniak,[3] A. Maisuradze,[2] E. Pomjakushina,[4] K. Conder,[4] V. Pomjakushin,[5] H. Luetkens,[2] S. Katrych,[6] A. Wisniewski,[3] R. Khasanov,[2] and H. Keller[1]

[1]*Physik-Institut der Universität Zürich, Winterthurerstrasse 190, CH-8057 Zürich, Switzerland*

[2]*Laboratory for Muon Spin Spectroscopy, Paul Scherrer Institute, CH-5232 Villigen PSI, Switzerland*

[3]*Institute of Physics, Polish Academy of Sciences, Aleja Lotników 32/46, PL-02-668 Warsaw, Poland*

[4]*Laboratory for Developments and Methods, Paul Scherrer Institute, CH-5232 Villigen PSI, Switzerland*

[5]*Laboratory for Neutron Scattering, ETHZ and PSI, CH-5232 Villigen PSI, Switzerland*

[6]*Laboratory for Solid State Physics, ETH Zurich, CH-8093 Zurich, Switzerland*

(Received 1 April 2010; revised manuscript received 8 June 2010; published 28 June 2010)

Iron-chalcogenide single crystals with the nominal composition $FeSe_{0.5}Te_{0.5}$ and a transition temperature of $T_c \simeq 14.6$ K were synthesized by the Bridgman method. The structural and anisotropic superconducting properties of those crystals were investigated by means of single crystal x-ray and neutron powder diffraction, superconducting quantum interference device and torque magnetometry, and muon-spin rotation (μSR). Room temperature neutron powder diffraction reveals that 95% of the crystal volume is of the same tetragonal structure as PbO. The structure refinement yields a stoichiometry of $Fe_{1.045}Se_{0.406}Te_{0.594}$. Additionally, a minor hexagonal Fe_7Se_8 impurity phase was identified. The magnetic penetration depth λ at zero temperature obtained by means of μSR was found to be $\lambda_{ab}(0)=491(8)$ nm in the *ab* plane and $\lambda_c(0)=1320(14)$ nm along the *c* axis. The zero-temperature value of the superfluid density $\rho_s(0) \propto \lambda^{-2}(0)$ obeys the empirical Uemura relation observed for various unconventional superconductors, including cuprates and iron pnictides. The temperature dependences of both λ_{ab} and λ_c are well described by a two-gap $s+s$-wave model with the zero-temperature gap values of $\Delta_S(0)=0.51(3)$ meV and $\Delta_L(0)=2.61(9)$ meV for the small and the large gap, respectively. The magnetic penetration depth anisotropy parameter $\gamma_\lambda(T)=\lambda_c(T)/\lambda_{ab}(T)$ increases with decreasing temperature, in agreement with $\gamma_\lambda(T)$ observed in the iron-pnictide superconductors.

DOI: 10.1103/PhysRevB.81.224520 PACS number(s): 74.25.Ha, 74.25.Op, 74.70.Xa, 76.75.+i

I. INTRODUCTION

Since the discovery of superconductivity in $LaFeAsO_{1-x}F_x$ (Ref. 1), high transition temperatures T_c up to 56 K were reported for several Fe-based superconductors with La substituted by other lanthanoids (*Ln*) including, e.g., Ce, Pr, Nd, Sm, and Gd.[2–6] Meanwhile, the family of Fe-based superconductors range from $LnFeAsO_{1-x}F_x$ (the so called "1111" family) over $AeFe_2As_2$ ("122", *Ae*=alkaline earth metal)[7] to the more simple LiFeAs ("111") (Ref. 8) and Fe*Ch* ("11", *Ch*=chalcogenide).[9] The Fe*Ch* system is especially similar to the FeAs-based superconductors, reflecting the ionic nature of the As and chalcogen atoms in these compounds.[10] Recently, two even more complicated families were discovered: the $(Fe_2As_2)(Ae_4M_2O_6)$ ("22426", *M*=transition metal) and the $(Fe_2As_2)(Ae_3M_2O_5)$ ("22325") systems.[11,12] If the parent compound is not already superconducting, superconductivity can be induced by charge carrier doping into either the Fe layers or the spacer layers as well as by applying external or internal pressure.[13–16]

Fe-based superconductors share some common properties with high-T_c cuprates such as a layered crystal structure, the presence of competing orders, a low carrier density, a small coherence length, and an unconventional pairing mechanism. On the other hand, there are some differences: the Fe-based superconductors have metallic parent compounds, the anisotropy is in general lower compared to that of the cuprates, and the order parameter symmetry is claimed to be $\pm s$-wave with Fermi-surface nesting playing a major role.[17–20] Hence, the fundamental question arises whether the mechanisms leading to superconductivity in both families of high-temperature superconductors (HTS) share a common origin.

Among the Fe-based superconductors the "11" system has attracted a lot of attention. The transition temperature T_c of $FeSe_{1-x}$ reaches values up to ≈37 K by applying hydrostatic pressure[9,21] and ≈14 K by partially substituting Se by the isovalent Te or S.[22] In $FeSe_xTe_{1-x}$ the antiferromagnetic order of FeTe is gradually suppressed by increasing *x* and superconductivity emerges with a maximal T_c at $x \simeq 0.5$.[16] Additionally, the "11" system has the simplest crystallographic structure among the Fe-based superconductors consisting of layers with a Fe square planar sheet tetrahedrally coordinated by *Ch*.[9] This and the similarity of the Fermi surface to the one of the FeAs-based superconductors[10] make the "11" system an ideal candidate to study the interplay of structure, magnetism, and superconductivity in Fe-based superconductors. In this paper we report on the structural and anisotropic superconducting properties of single crystals with the nominal composition of $FeSe_{0.5}Te_{0.5}$ that were studied by x-ray and neutron powder diffraction, superconducting quantum interference device (SQUID), and torque magnetometry as well as muon-spin rotation (μSR). A part of the present results are in agreement with the findings of a recent μSR study performed on a polycrystalline sample of $FeSe_{0.5}Te_{0.5}$.[23]

II. EXPERIMENTAL DETAILS

A. Single crystal growth

Single crystals with the nominal composition of $FeSe_{0.5}Te_{0.5}$ were grown by the Bridgman method, similar to

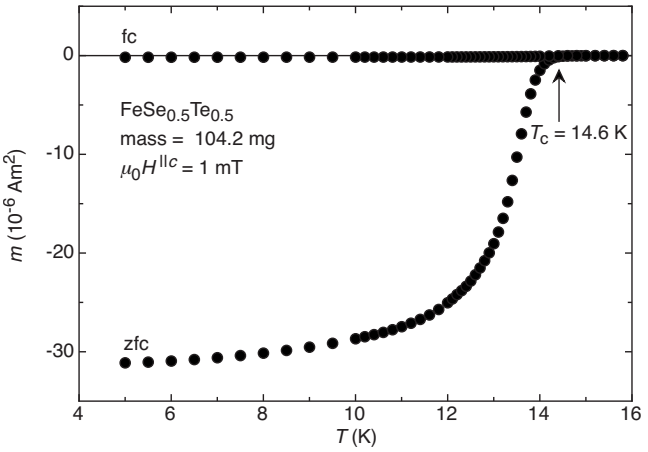

FIG. 1. Magnetic moment m as a function of temperature T in a magnetic field of 1 mT applied parallel to the c axis of single crystal $FeSe_{0.5}Te_{0.5}$, recorded in the Meissner state in zfc mode and in fc mode. The onset transition temperature $T_c \simeq 14.6$ K (vertical arrow) is characteristic for optimal doping $x \simeq 0.5$ of $FeSe_xTe_{1-x}$.

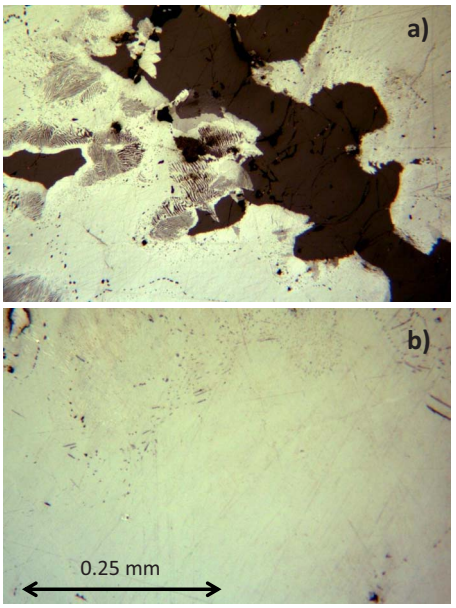

FIG. 2. (Color online) Polarized light microscopic photographs of polished surfaces of the $FeSe_{0.5}Te_{0.5}$ crystal. (a) Microphotography of the crystal surface cut perpendicular to the cleaving facet. Domains with different crystallographic orientations and/or different phases are visible. (b) Micrography of the resulting polished cleaving facet.

that reported by Sales *et al.*[22] Appropriate amounts of Fe, Se, and Te powders with a minimum purity of 99.99 % were mixed together, pressed into a rod (diameter 7 mm), and then evacuated and sealed in a double-wall quartz ampoule for air protection. The ampoule was placed into a vertical furnace with a temperature gradient and annealed at 1200 °C for 4 h. Afterwards the samples were cooled down with a rate of 4 °C/h to 750 °C, followed by a quick cooling (50 °C/h) to room temperature. The so-obtained crystals were easily cleaved from the as-grown crystal along the *ab* plane (cleaving facet).

Figure 1 presents a low-field measurement of the magnetic moment m in a magnetic field of $\mu_0 H = 1$ mT applied along the c axis performed in zero-field-cooled (zfc) and field-cooled (fc) mode. The sample exhibits a clear transition to the superconducting state with an onset transition temperature of $T_c \simeq 14.6$ K. The signal magnitude obtained in the zfc mode reflects a full diamagnetic response of the sample with a calculated susceptibility of $\chi \approx -1$ at $T = 0$ K. The density ρ and the demagnetization factor D were estimated to $\rho = 6.04$ g/cm^3 and $D \approx 0.55$, respectively. Note that a similar result was already observed for a sample of the same batch.[16] The low value of the fc signal indicates strong pinning.

The surface of the as-grown crystal was polished and the surface morphology was examined in a polarized light microscope. Figure 2(a) shows a microphotography of the crystal surface cut perpendicular to the cleaving facet. Distinct domains of different crystallographic orientations and/or different phases are observed. Figure 2(b) shows the polished cleaving facet. No orientation misfit is observed here. In conclusion, the main phase in the material is textured with the c axis perpendicular to the cleaving facet whereas the a and b axes are oriented within domains of irregular shape.

B. Crystal structure

The crystal structure and the phase purity were checked using a single-crystal x-ray diffractometer equipped with a charged-coupled device detector (Xcalibur PX, *Oxford Diffraction*, sample-detector distance 60 mm). Crystallites with approximate dimensions of $1 \times 1 \times 0.2$ mm^3 were cleaved from the as-grown crystal for the single-crystal x-ray diffraction studies. The single crystal diffractographs are shown in Fig. 3. Two distinct crystallographic phases were identified. The major phase of the crystal exhibits a tetragonal lattice [space group: $P4/nmm$ and lattice parameters: $a = 3.7980(2)$ Å and $c = 6.038(1)$ Å]. The reconstruction of the reciprocal space sections of the studied plate-like crystals shows pronounced mosaic spreads with an average mosaicity on the order of about 4°. A small part of the studied crystals with polygonal structure exhibits a hexagonal lattice structure, which is associated with an impurity phase.

Detailed crystal-structure investigations were completed by means of neutron powder diffraction (NPD) at the neutron spallation source SINQ at the Paul Scherrer Institute (PSI, Switzerland) using the High-Resolution Powder diffractometer for Thermal neutrons (HRPT) (Ref. 24), with a neutron wavelength of $\lambda_n = 1.494$ Å. For these experiments, a part of the crystal with the nominal composition of $FeSe_{0.5}Te_{0.5}$ was cleaved, powderized, and loaded into the sample holder in a He-glove box to protect the powder from oxidation. Room-temperature NPD experiments revealed that the sample consists mainly of the tetragonal phase (space group $P4/nmm$) of the PbO type which becomes orthorhomic and superconducting at low temperatures. The results of the Rietveld refinement of the NPD spectra performed with the program FULLPROF (Ref. 25) are shown in Fig. 4. For the refinement it was assumed that all Fe sites are occupied. Additionally, a preferred orientation was assumed as small plate-like grains are created during the pow-

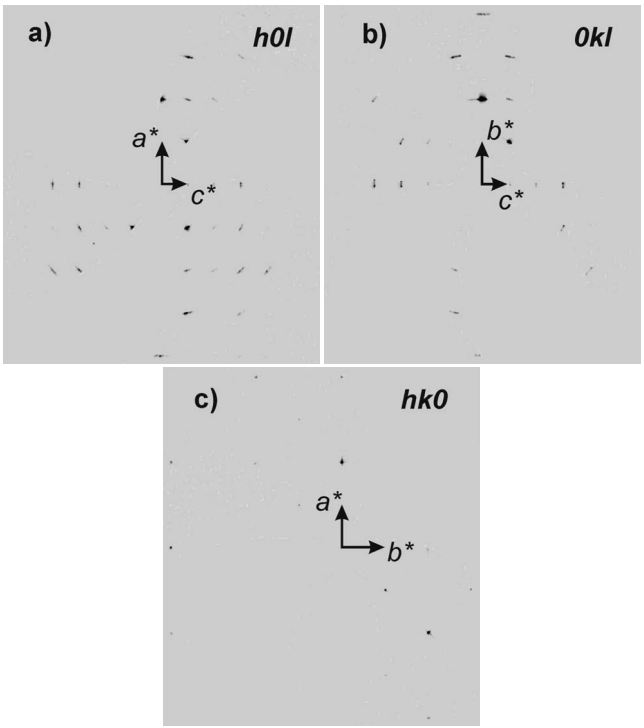

FIG. 3. The reciprocal space sections of the $FeSe_{0.5}Te_{0.5}$ crystal: (a) *h0l* reciprocal layer, (b) 0*kl* reciprocal layer, and (c) *hk*0 reciprocal layer.

derization process. The refined stoichiometry is $Fe_{1.045}Se_{0.406(16)}Te_{0.594(16)}$ [a=3.8028(1) Å and c =6.0524(3) Å]. Note that these values were obtained by assuming a texture in the powder sample. As impurity phases hexagonal Fe_7Se_8 (space group $P6_3/mmc$, 5.35(40)% volume fraction) and elemental Fe ($\leq$1%) were identified.

It was shown that in the β-phase additional excess Fe occupies interstitial lattice sites.[26,27] However, introduction of interstitial Fe atoms in the refinement of the data did not

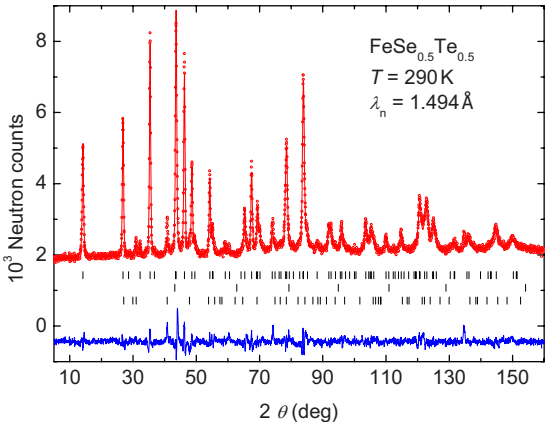

FIG. 4. (Color online) Rietveld refinement pattern (upper–red) and difference plot (lower–blue) of the neutron diffraction data for the crystal with the nominal composition of $FeSe_{0.5}Te_{0.5}$. The rows of ticks show the Bragg peak positions for the main phase and two impurity phases. The refined stoichiometry of the main tetragonal phase is $Fe_{1.045}Se_{0.406}Te_{0.594}$ (see text for details).

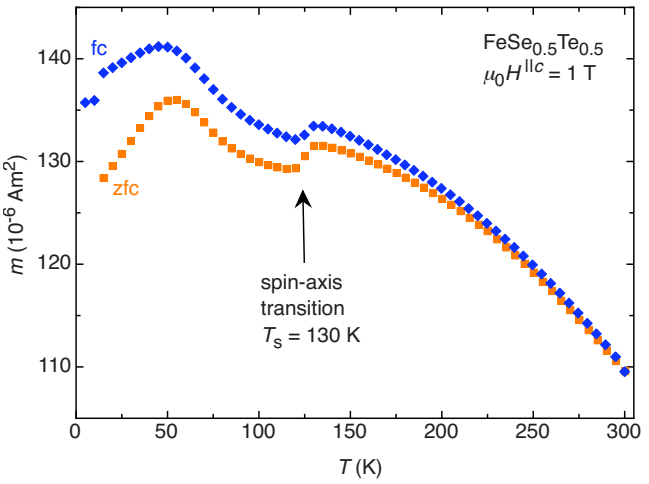

FIG. 5. (Color online) Temperature dependence of the magnetic moment measured in zfc and fc modes in a magnetic field of 1 T applied parallel to the c axis of the crystal with nominal composition $FeSe_{0.5}Te_{0.5}$.

improve the fit. This suggests the presence of only a very small amount of such defects, in agreement with the model that in isostructural $FeSe_{1-x}$ (Ref. 28) no interstitial Fe is present. This is in contrast to FeTe where interstitial Fe atoms were detected.[26,27]

The existence of an impurity phase of Fe_7Se_8 in the studied crystal was confirmed by magnetization measurements. Figure 5 shows the temperature dependence of the magnetic moment recorded for a $FeSe_{0.5}Te_{0.5}$ crystal (mass ~200 mg) in a magnetic field of 1 T, applied parallel to the c axis of the crystal. Fe_7Se_8 is known to undergo a spin-axis transition at 130 K leading to a reduction in magnetization for H parallel to the c axis,[29] as observed in the studied sample (Fig. 5).

III. MAGNETIC PROPERTIES

A. Magnetization measurements

The magnetic properties of the crystals were investigated by a commercial *Quantum Design* 7-T magnetic property measurement system XL SQUID magnetometer at temperatures ranging from 2 K to 300 K and in magnetic fields from 0 T to 7 T using the reciprocating sample option. Magnetic torque measurements were performed with a commercial *Quantum Design* 9-T physical property measurement system equipped with a magnetic torque option.

The magnetization of $FeSe_{0.5}Te_{0.5}$ was measured on a crystal with a mass of the order of 200 mg. The Meissner fraction derived from the magnetic moment in the fc mode as compared to the one from zfc mode is estimated to be ~1% in 1 mT (Fig. 1). This indicates strong vortex pinning in agreement with the weakly field-dependent and pronounced critical current density and with the significant irreversibility in the magnetic torque experiments already present slightly below T_c (as discussed later, Fig. 8). Using Bean's model,[30,31] magnetization hysteresis loop measurements allow to estimate the superconducting critical current density of the order of 10^7 A/m^2. The presence of impurity phases

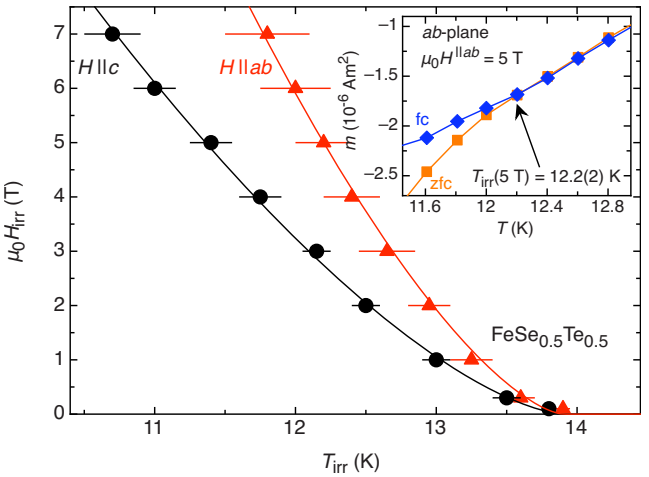

FIG. 6. (Color online) Irreversibility line $H_{irr}(T)$ derived from SQUID measurements for two field configurations, H parallel to the c axis and H parallel to the ab plane of the $FeSe_{0.5}Te_{0.5}$ crystal. The solid black and red lines correspond to fits using the power-law $(1-T/T_c)^n$ with an exponent $n \simeq 1.5$. The inset illustrates how T_{irr} was determined. The lines are guides to the eyes.

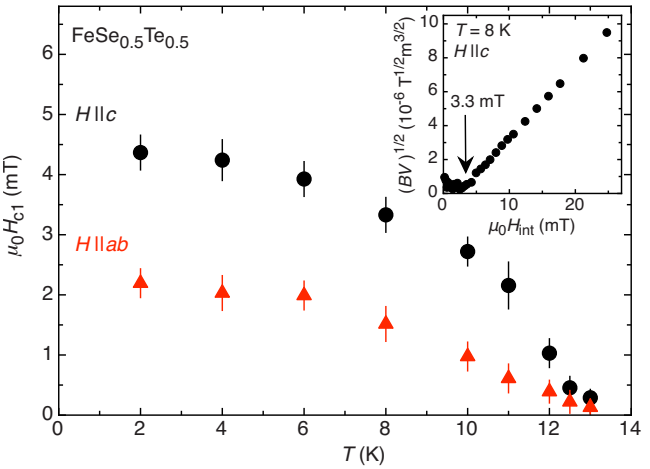

FIG. 7. (Color online) H_{c1} as a function of temperature for both orientations H parallel to the c axis and H parallel to the ab plane for single crystal $FeSe_{0.5}Te_{0.5}$. The inset illustrates the deviation from the linear $B^{1/2}(H)$ dependence plotted as $(BV)^{1/2}$ vs $\mu_0 H_{int}$.

lowers the transport current density as phase separation boundaries prevent to develop a global circulating current. This leads to a relatively low value of the estimated critical-current density as compared to those observed in monocrystalline iron pnictides.[17]

From temperature-dependent magnetization measurements at various magnetic fields the irreversibility line $H_{irr}(T)$ was deduced by following the temperatures for which the zfc and fc branches of the magnetic moment merge. This derivation of $H_{irr}(T)$ is not influenced by the presence of Fe_7Se_8 impurities in the studied samples. Although, the data presented in Fig. 5 indicate that the zfc and fc curves merge only above 200 K, this impurity effect does not affect the determination of T_{irr} here since the temperature range for probing the superconducting irreversibility did not exceed 20 K. No difference between zfc and fc curves, recorded for all magnetic fields in both field configurations, was visible in the temperature range between T_c and maximum applied temperature (inset to Fig. 6). Thus, the influence of an additional phase in the studied samples on the determination of the irreversibility temperature is negligible. The results are presented in Fig. 6, where the inset to the figure illustrates the derivation of T_{irr} in a magnetic field of 5 T parallel to the ab plane. The data were analyzed using the power-law $(1-T/T_c)^n$ with $n \simeq 1.5$, typical for cuprate HTS.[32] The irreversibility line $H_{irr}(T)$ is located at relatively high magnetic fields. Interestingly, H_{irr} is for H parallel to the ab plane almost overlapping, in the studied field range, with the values of the upper critical field $H_{c2}^{\|c}$ reported by Fang *et al.*[33]

The temperature dependence of the lower critical field H_{c1} was studied by following the field H_{c1}^*, where the first vortices start to penetrate the sample at its surface, which is directly related to H_{c1}. The field dependence of the magnetization was measured at different temperatures for the magnetic field parallel to the ab plane and parallel to the c axis of the sample. For a given shape of the investigated crystal, the demagnetizing factors D were calculated for the magnetic field applied along all of the crystallographic axis. The variation of magnetic induction $B=\mu_0(m/V+H_{int})$ as a function of the internal magnetic field $H_{int}=H_{ext}-DM$ (H_{ext} denotes the external magnetic field) is presented in the inset of Fig. 7. The lower critical fields for H parallel to the ab plane and parallel to the c axis presented in Fig. 7 were determined as the field where the magnetization deviates from the linear behavior. For the case of weak bulk pinning, surface barriers may play a crucial role and determine the first field of flux penetration and the irreversibility line.[34–36] The impact of surface barriers leads to asymmetric $M(H)$ loops. The descending branch is in such a case almost horizontal. For our samples, however, we observe symmetric magnetization loops which means that the bulk pinning controls mainly the entry and exit of the magnetic flux. From these data, the zero-temperature values were found to be $\mu_0 H_{c1}^{\|ab}(0) = 2.0(2)$ mT and $\mu_0 H_{c1}^{\|c}(0) = 4.5(3)$ mT. In order to extract the values of the magnetic penetration depth from the measured values of H_{c1} the following basic relations were applied:[37]

$$H_{c1}^{\|c} = \frac{\Phi_0}{8\pi\mu_0\lambda_{ab}^2}\left[2\ln\left(\frac{\lambda_{ab}}{\xi_{ab}}\right)+1\right], \quad (1)$$

$$H_{c1}^{\|ab} = \frac{\Phi_0}{8\pi\mu_0\lambda_{ab}\lambda_c}\left[\ln\left(\frac{\lambda_{ab}\lambda_c}{\xi_{ab}\xi_c}\right)+1\right]. \quad (2)$$

Here, λ_{ab} and λ_c are the magnetic penetration depths parallel to the ab plane and to the c axis, respectively, ξ_{ab} and ξ_c the corresponding coherence lengths, Φ_0 is the elementary flux quantum, and μ_0 the magnetic constant. The values of ξ_{ab} and ξ_c were derived from $H_{c2}^{\|ab}$ and $H_{c2}^{\|c}$ measurements and found to be approximately 2.8 nm at zero temperature for both field configurations.[33,38] The following zero-temperature values of magnetic penetration depths were obtained: $\lambda_{ab}(0) \simeq 460(100)$ nm and $\lambda_c(0) \simeq 1100(300)$ nm. These values are in good agreement with the values deter-

TABLE I. Summary of the parameters obtained for single crystal $FeSe_{0.5}Te_{0.5}$ by means of μSR and magnetization measurements. The errors of the μSR data are statistical errors and do not take into account for any systematical errors that may be present in the data. Symbol w is defined in the description of Eq. (7).

	μSR		Magnetization	
	ab plane	*c* axis	*ab* plane	*c* axis
T_c (K)	14.1(1)		14.6(1)	
Δ_S^0 (meV)	0.51(3)			
$2\Delta_S^0/k_BT_c$	0.84(4)			
Δ_L^0 (meV)	2.61(9)			
$2\Delta_L^0/k_BT_c$	4.3(1)			
w	0.32(1)	0.36(2)		
$\lambda_{ab,\ c}(0)$ (nm)	491(8)	1320(14)	460(100)	1100(300)
μ_0H_{c1} (mT)			2.0(2)	4.5(3)

mined by μSR discussed below (see Table I).

In order to quantify the anisotropy of superconducting state parameters, magnetic torque studies were performed close to T_c, where irreversibility effects are small. The measurements on small crystals ($\sim 1\times 1\times 0.2$ mm^3) revealed a clear superconducting response, but unfortunately, due to the small amplitude of the superconducting torque signal in the mixed state close to T_c, a relatively strong background component of magnetic origin contributes significantly to the torque signal. The magnetic background signal in the superconducting state is confirmed by following the torque to temperatures above T_c. In order to exclude artifacts in the subsequent analysis, all background components within the superconducting state were subtracted from the torque prior to the analysis (see below). To minimize the influence of pinning the mean reversible torque $\tau_{rev}=[\tau(\theta^+)+\tau(\theta^-)]/2$ was derived from measurements with clockwise and counterclockwise rotating the sample in the field. The superconducting anisotropy parameter $\gamma=\lambda_c/\lambda_{ab}$ may be extracted from the measured torque $\tau(\theta)$ using the relation[39,40]

$$\tau(\theta) = -\frac{V\Phi_0 H}{16\pi\lambda_{ab}^2}\left(1-\frac{1}{\gamma^2}\right)\frac{\sin(2\theta)}{\epsilon(\theta)}\ln\left[\frac{\eta H_{c2}^{\|c}}{\epsilon(\theta)H}\right] + A_\tau \sin(2\theta), \tag{3}$$

where V is the volume of the crystal, λ_{ab} is the in-plane component of the magnetic penetration depth, $H_{c2}^{\|c}$ is the upper critical field along the c axis of the crystal, η denotes a numerical parameter of the order of unity depending on the structure of the flux-line lattice, A_τ is the amplitude of the background torque, and $\epsilon(\theta)=[\cos^2(\theta)+\gamma^{-2}\sin^2(\theta)]^{1/2}$. Since Eq. (3) contains multiple correlated parameters, making a simultaneous fit of all quantities difficult, all $H_{c2}^{\|c}$ values were fixed to those reported in Ref. 33 during the fitting procedure by neglecting any influence of the parameter η. Because the magnetic background contributions tend to influence and alter the fitting parameter $H_{c2}^{\|c}$ strongly,[41,42] the data were fitted by Eq. (3) using the symmetrized expression for the torque $\tau_{symm}(\theta)=\tau(\theta)+\tau(\theta+90°)$.[43] The result of this analysis is depicted in Fig. 8, yielding an anisotropy parameter $\gamma=3.1(4)$ in the vicinity of T_c.

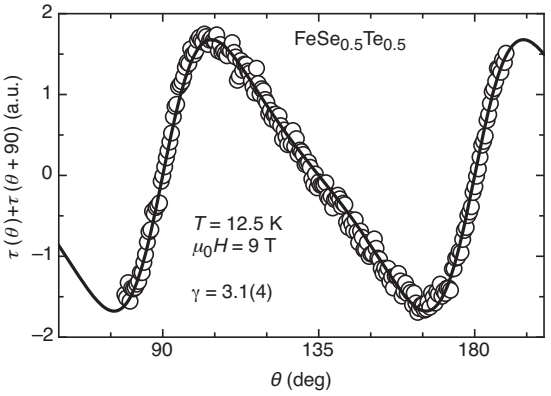

FIG. 8. Symmetrized torque τ_{symm} for the studied crystal of $FeSe_{0.5}Te_{0.5}$ in the superconducting state as a function of the angle θ. The torque data are well described by Eq. (3), yielding an anisotropy parameter $\gamma=3.1(4)$ close to T_c.

B. Muon-spin rotation

μSR is a direct and bulk sensitive probe to investigate local magnetic fields in magnetic solids.[44] Nearly 100% spin-polarized positive muons μ^+ are implanted into the sample and stop at interstitial lattice sites, where the muon spins precess around the local magnetic field B with the Larmor frequency $\omega_L=\gamma_\mu B$ ($\gamma_\mu/2\pi=135.5$ MHz/T is the muon gyromagnetic ratio). At the stopping site the muon acts as a magnetic micro probe and measures the internal field distribution. Within the muon's lifetime of $\tau=2.2$ μs it decays into two neutrinos and a positron, which is emitted predominantly along the muon spin polarization at the moment of decay. The direction of the emitted decay positron and the time between the muon implantation and its decay is measured for typically 10^6 positrons. This way the time evolution of the muon spin polarization $P(t)$ is obtained. Zero-field (ZF) μSR experiments probe the magnetic state of a material as the muon spins precess only around the internal field without applying an external magnetic field. In transverse field (TF) μSR experiments, the local magnetic field at the muon site in the sample is probed in the presence of an external magnetic field perpendicular to the initial muon spin polarization. TF μSR is a very powerful tool to investigate the local magnetic field distribution in the vortex state of type-II superconductors. A comprehensive review of the application of μSR to the study of superconductors can be found in Ref. 44.

The μSR experiments were carried out at the πM3 beam line at the Swiss Muon Source (SμS) at PSI. ZF and TF μSR experiments were performed in a temperature range from 1.5 to 20 K. The TF experiments were carried out in two sets of measurements when the external field $\mu_0H=11.8$ mT was applied either parallel to the crystallographic c axis or parallel to the ab plane.

The ZF μSR spectra obtained at 1.6 K and above T_c show no difference [Fig. 9(a)]. This indicates that the magnetic state of $FeSe_{0.5}Te_{0.5}$ below and above T_c is the same. The

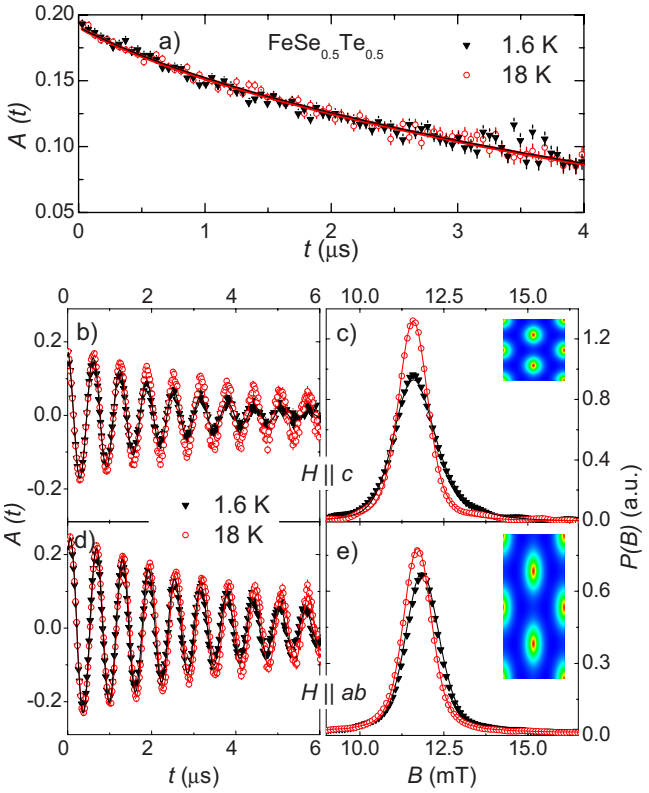

FIG. 9. (Color online) (a) ZF μSR time spectra for $FeSe_{0.5}Te_{0.5}$ recorded at 1.6 K and above T_c. The solid lines represent fits using Eq. (4). [(b) and (d)] TF μSR time spectra for H parallel to the c axis and H parallel to the ab plane, taken at 1.6 K and above T_c. [(c) and (e)] The corresponding magnetic field distributions $P(B)$. The solid lines represent fits using Eq. (5). The insets show the counter plots of the local field variation at 1.6 K, (c) $\lambda_a=\lambda_b$ and (e) $\lambda_c=2.7\lambda_{ab}$.

solid lines in Fig. 9(a) correspond to fits using an exponential decay of the initial muon-spin polarization

$$A^{\mathrm{ZF}}(t) = A_{\mathrm{SC}} \cdot e^{-\Lambda t} + A_{\mathrm{bg}} e^{-\Lambda_{\mathrm{bg}} t}. \tag{4}$$

Here, A_{SC} is the asymmetry of the superconducting phase and Λ is the corresponding depolarization rate. The temperature-independent background signal A_{bg}, arising from the Fe_7Se_8 impurity phase was fixed to 6% of the total asymmetry during the fit, corresponding to the results of the NPD refinement. The exponential character of the muon-spin depolarization is typical for diluted and randomly distributed magnetic moments that are static on the muon time scale as shown in Ref. 45.

In the TF geometry muons probe the magnetic field distribution $P(B)$ in the sample. In the mixed state of a type-II superconductor $P(B)$ is determined by the magnetic penetration depth λ and the coherence length ξ. The $P(B)$ distributions obtained from the Fourier transform of the μSR time spectra [Figs. 9(b) and 9(d)] at 1.6 K and above T_c are shown in Figs. 9(c) and 9(e). In the normal state a symmetric $P(B)$ at the position of the applied magnetic field is observed. The broadening of $P(B)$ in the normal state is due to nuclear and diluted electronic magnetic moments. Below T_c an additional

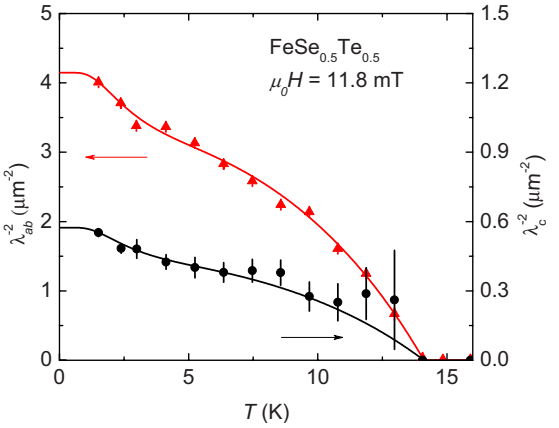

FIG. 10. (Color online) Temperature dependence of the penetration depth components λ_{ab} and λ_c of single crystal $FeSe_{0.5}Te_{0.5}$. The solid lines correspond to fits using Eq. (7). The corresponding fit parameters are listed in Table I.

broadening and an asymmetric line shape $P(B)$ due to the formation of the flux line lattice (FLL) show up. The TF μSR time spectra were analyzed by a theoretical polarization function $A(t)$ by assuming an internal field distribution $P_{\mathrm{FLL}}(B)$ and to account for the FLL disorder by multiplying $P_{\mathrm{FLL}}(B)$ with a Gaussian function[46,47]

$$A(t) = A_0 e^{i\phi} e^{-(\sigma_g^2+\sigma_{nm}^2)t^2/2-\Lambda_e t} \int P_{\mathrm{FLL}}(B) e^{i\gamma_\mu B t} dB. \tag{5}$$

Here, A_0 and ϕ are the initial asymmetry and the phase of the muon-spin ensemble, respectively, σ_g is a parameter related to the FLL disorder,[46,47] σ_{nm} is the nuclear moment contribution measured at $T>T_c$, which is generally temperature independent,[48] and Λ_e is the relaxation rate of the electronic moment contribution, which was obtained from the measurements taken above T_c.

The magnetic field distribution $P_{\mathrm{FLL}}(B)$ for a FLL of an anisotropic superconductor was determined from the spatial variation in the magnetic field $B(\mathbf{r})$ calculated in an orthogonal frame x, y, and z with $H\|z$ (z is one of the principal axes a, b, and c) using the expression[49]

$$B(\mathbf{r}) = \langle B \rangle \sum_G \exp(-i\mathbf{G}\cdot\mathbf{r}) B_{\mathbf{G}}(\lambda, \xi, b). \tag{6}$$

Here, $\langle B\rangle$ is the average magnetic field in the superconductor (magnetic induction), $b=\langle B\rangle/B_{c2}$ the reduced field ($B_{c2}=\mu_0 H_{c2}$), and $\mathbf{r}$ the vector coordinate in a plane perpendicular to the applied field. The Fourier components $B_{\mathbf{G}}$ were obtained within the framework of the Ginzburg-Landau model.[49] For a detailed description of the fitting procedure we refer to Ref. 47. The solid lines in Figs. 9(c) and 9(e) correspond to the fast Fourier transforms of the described fits to the μSR time spectra.

The temperature dependences of λ_{ab}^{-2} and λ_c^{-2} extracted from the μSR time spectra using the fitting procedure described above are shown in Fig. 10. These data were analyzed within the framework of the phenomenological α model[50] by assuming that λ^{-2} is a linear combination of two terms

$$\frac{\lambda^{-2}(T)}{\lambda^{-2}(0)} = w\frac{\lambda^{-2}(T,\Delta_S^0)}{\lambda^{-2}(0,\Delta_S^0)} + (1-w)\frac{\lambda^{-2}(T,\Delta_L^0)}{\lambda^{-2}(0,\Delta_L^0)}. \quad (7)$$

Here, Δ_S^0 and Δ_L^0 are the zero-temperature values of the small and the large gap, respectively, and w $(0 \leq w \leq 1)$ is the weighting factor which measures the relative contribution of the two gaps to $\lambda^{-2}(T)/\lambda^{-2}(0)$. For the temperature dependence of λ^{-2} of a London superconductor $(\lambda \gg \xi)$ with a *s*-wave gap the following relation can be used:[37]

$$\frac{\lambda^{-2}(T,\Delta_{S(L)}^0)}{\lambda^{-2}(0,\Delta_{S(L)}^0)} = 1 + 2\int_{\Delta(T)}^{\infty}\left(\frac{\partial f}{\partial E}\right)\frac{E}{\sqrt{E^2-\Delta^2(T)}}dE. \quad (8)$$

Here, $\lambda(0)$ is the zero-temperature value of the magnetic penetration depth, $f(E)=[1+\exp(E/k_BT)]^{-1}$ is the Fermi function (E is the excitation energy, k_B is the Boltzmann constant), and $\Delta(T)=\Delta(0)\tilde{\Delta}(T/T_c)$ represents the temperature dependence of the gap with $\tilde{\Delta}(T/T_c) = \tanh(1.82[1.018(T_c/T-1)^{0.51}])$.[50] Note that this phenomenological model is only applicable for superconductors in the clean limit.[51] Recent magnetization and resistivity experiments performed on single crystals of $Fe_{1+\delta}Se_{1-x}Te_x$ $(0 \leq x < 1)$ indicate that these superconductors are in the clean limit.[52]

The ratios $2\Delta_S^0/k_BT_c=0.84(4)$ and $2\Delta_L^0/k_BT_c=4.3(1)$ are close to what was reported for isostructural $FeSe_{1-x}$.[45] Based on scanning tunneling spectroscopy measurements, Kato *et al.*[53] reported for $FeSe_{0.4}Te_{0.6}$ only one *s*-wave gap $\Delta \simeq 2.3$ meV. This value is quite similar to our result of the large gap $[\Delta_L^0=2.61(9)$ meV]. However, a single *s*-wave gap is not sufficient to describe the present μSR data. The weighting factors w are about the same for $1/\lambda_{ab}^2$ and $1/\lambda_c^2$. Similar results were already reported for isostructural $FeSe_{1-x}$.[45] Recently, Kim *et al.*[54] reported on magnetic penetration depth measurements on $Fe_{1.03}Se_{0.37}Te_{0.63}$ by means of a radio-frequency tunnel diode resonator technique. Their value $\lambda_{ab}(0) \simeq 560(20)$ nm is in good agreement with the value reported here (see Table I). Furthermore, they found a clear signature of multigap superconductivity with comparable gap values ($\Delta_S^0 \simeq 1.2$ meV and $\Delta_L^0 \simeq 2$ meV). In a recent μSR study of polycrystalline $FeSe_{0.5}Te_{0.5}$ the temperature dependence of λ_{ab} was found to be compatible with either a two gap *s*+*s*-wave or anisotropic *s*-wave model with $\lambda_{ab}=534(2)$ nm.[23] For the *s*+*s*-wave analysis, the following results were obtained: $\Delta_L(0)=2.6(1)$ meV, $\Delta_S(0)=0.87(6)$ meV, and $1-w=0.70(3)$.[23] These results are in fair agreement with the present results listed in Table I.

Uemura *et al.*[55] found an empirical relation between the zero-temperature superfluid density $\rho_s(0) \propto \lambda_{ab}^{-2}(0)$ and T_c which seems to be generic for various families of cuprate HTS (Uemura plot). This "universal" relation $T_c(\rho_s)$ has the following features: with increasing carrier doping T_c initially increases linearly $[T_c \propto \rho_s(0)]$, then saturates, and finally is suppressed for high carrier doping. It is interesting to check whether the Uemura relation also holds for iron-based superconductors. For this reason, T_c vs $\lambda_{ab}^{-2}(0)$ is plotted in Fig. 11 for a selection of various Fe-based superconductors investigated so far.[13,14,45,54,57–63] For comparison the linear parts of the Uemura relation for hole-doped (dashed line) and electron-doped (dotted line) cuprate HTS are also shown in Fig. 11. Due to the small number of data points available for a particular family of Fe-based superconductors there is no obvious trend visible. However, all data points are located within an area determined by the straight lines representing the hole-doped and electron-doped cuprates. Whereas several of the Fe-based HTS, including $FeSe_{0.5}Te_{0.5}$ (red star in Fig. 11) investigated here, are located near the hole-doped cuprates in the Uemura plot, the "111" system appears to be close to the electron-doped cuprates.

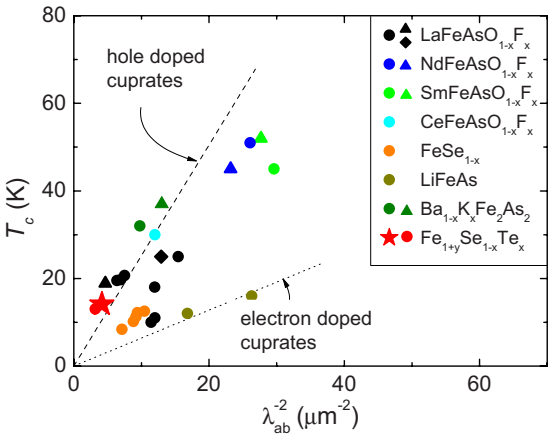

FIG. 11. (Color online) Uemura plot for a selection of some Fe-based HTS. The Uemura relation observed for underdoped cuprates is included for comparison as a dashed line for hole doping and as a dotted line for electron doping (after Ref. 56). $LaFeAsO_{1-x}F_x$ data from Refs. 13 and 57 (●), Ref. 58 (▲), and Ref. 59 (◆); $NdFeAsO_{1-x}F_x$ data from Ref. 60 (●) and Ref. 59 (▲); $SmFeAsO_{1-x}F_x$ data from Ref. 60 (●) and Ref. 14 (▲); $CeFeAsO_{1-x}F_x$ data from Ref. 59, $FeSe_{1-x}$ data from Refs. 45 and 61, LiFeAs data from Ref. 62, $Ba_{1-x}K_xFeAs$ data from Ref. 63, and $Fe_{1+y}Se_{1-x}Te_x$ data from Ref. 54 (●). The red star (★) is showing the data for $FeSe_{0.5}Te_{0.5}$ obtained in this work.

IV. TEMPERATURE-DEPENDENT ANISOTROPY PARAMETERS

For a conventional single-band *s*-wave-layered superconductor, the anisotropy parameter is defined as[37]

$$\gamma = \sqrt{m_c^*/m_{ab}^*} = \lambda_c/\lambda_{ab} = H_{c2}^{\parallel ab}/H_{c2}^{\parallel c} = \xi_{ab}/\xi_c. \quad (9)$$

Here, m_{ab}^* and m_c^* are the effective charge carrier masses related to supercurrents flowing in the *ab* planes and along the *c* axis, respectively. Whereas the cuprates were characterized by a well-defined effective mass anisotropy, the observation of two distinct anisotropy parameters in MgB_2 challenged the understanding of anisotropic superconductors.[64–66] Various experiments, such as magnetic torque,[41,42] tunneling,[67,68] point contact and infrared spectroscopy,[69,70] as well as the measurements of the specific heat,[71] the lower and upper critical field,[72,73] and the superfluid density[45,63,74–77] indicate that Fe-based pnictides are multigap superconductors having unconventional anisotropic properties,[41–43] similar to MgB_2.[78,79]

The temperature dependence of the magnetic penetration depth anisotropy parameter $\gamma_\lambda=\lambda_c/\lambda_{ab}$ extracted from the

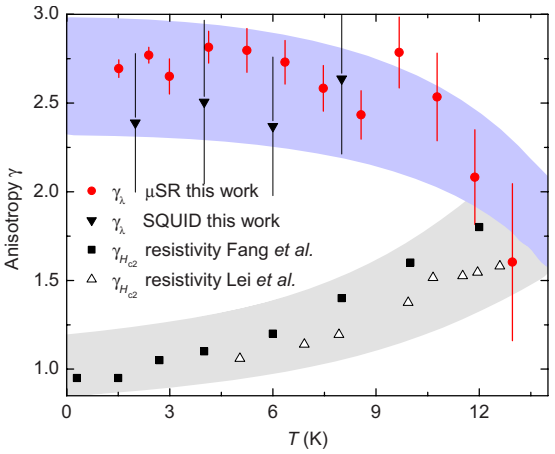

FIG. 12. (Color online) Comparison of the temperature dependence of the magnetic penetration depth anisotropy parameter $\gamma_\lambda = \lambda_c/\lambda_{ab}$ measured by μSR and by SQUID for single crystal $FeSe_{0.5}Te_{0.5}$ with the H_{c2}-anisotropy parameter $\gamma_{H_{c2}} = H_{c2}^{\|ab}/H_{c2}^{\|c}$ obtained from resistivity measurements for $Fe_{1.11}Se_{0.4}Te_{0.6}$ by Fang *et al.* (Ref. 33) and for $Fe_{1.02}Se_{0.39}Te_{0.61}$ by Lei *et al.* (Ref. 38). The lines are guides to the eyes.

μSR data (see Fig. 10) is shown in Fig. 12. Note that γ_λ increases with decreasing temperature and saturates at $\gamma_\lambda \simeq 2.6(3)$ at low temperatures. This observation is further supported by the temperature dependence of γ_λ determined from the lower critical field measurements presented in Fig. 7. In this case γ_λ is readily obtained from Eqs. (1) and (2) (Ref. 37)

$$\gamma_\lambda = \frac{\lambda_c}{\lambda_{ab}} = \frac{H_{c1}^{\|c}}{H_{c1}^{\|ab}}\left(1 + \frac{\ln(\gamma_\lambda) + \ln(\gamma_{H_{c2}})}{2\ln(\kappa_{ab}) + 1}\right). \quad (10)$$

Here, $\kappa_{ab} = \lambda_{ab}/\xi_{ab}$ denotes the Ginzburg-Landau parameter. In this work, κ_{ab} was estimated to be $\simeq 180$ from present experiments.[33] The values of γ_λ extracted from the SQUID data using Eq. (10) are also depicted in Fig. 12 and are in fair agreement with those obtained from the μSR data.

The upper critical field anisotropy parameter, $\gamma_{H_{c2}} = H_{c2}^{\|ab}/H_{c2}^{\|c} = \xi_{ab}/\xi_c$, was studied by Fang *et al.*[33] and Lei *et al.*[38] by resistivity measurements on $Fe_{1+y}Se_{0.4}Te_{0.6}$ ($y = 0.02$ and 0.11). These data are plotted in Fig. 12 as well. Note that $\gamma_{H_{c2}}$ decreases with decreasing temperature. Obviously, the behavior of the two distinct anisotropy parameters γ_λ and $\gamma_{H_{c2}}$ is *not* consistent with Eq. (9). The observed behavior is similar to the one of the two-gap superconductor MgB_2 and other Fe-based superconductors.[42] For MgB_2, however, γ_λ decreases with decreasing temperature while $\gamma_{H_{c2}}$ increases.[65]

V. CONCLUSIONS

Single crystals with a nominal composition of $FeSe_{0.5}Te_{0.5}$ were studied by means of μSR, SQUID and torque magnetometry, and neutron powder diffraction. At room temperature the crystal shows mainly a tetragonal phase of PbO type that becomes orthorombic and superconducting at low temperatures. The stoichiometry was refined to $Fe_{1.045}Se_{0.406}Te_{0.594}$. The onset transition temperature is $T_c = 14.6$ K, and the lower critical field values measured for both crystallographic directions were determined at zero temperature as $H_{c1}^{\|ab}(0) = 2.0(2)$ mT and $H_{c1}^{\|c}(0) = 4.5(3)$ mT.

By means of μSR it was found that for $FeSe_{0.5}Te_{0.5}$ the temperature dependence of the magnetic penetration depth for both crystallographic directions is best described by a two gap $s+s$-wave model with zero-temperature values of the magnetic penetration depth of $\lambda_{ab}(0) = 491(8)$ nm and $\lambda_c(0) = 1320(14)$ nm, consistent with recent μSR results obtained for a polycrystalline sample.[23] This two-gap scenario is in line with the generally accepted view of multigap superconductivity in Fe-based HTS. Evtushinsky *et al.*[80] pointed out that most Fe-based HTS exhibit two gaps, a large one with $2\Delta/k_BT_c = 7(2)$ and a small one with 2.5(1.5). The magnitudes of the large and the small gap for $FeSe_{0.5}Te_{0.5}$ [$2\Delta_S/k_BT_c = 0.84(4)$ and $2\Delta_L/k_BT_c = 4.3(1)$] are at the lower limit for Fe-based HTS. Moreover, the magnetic penetration depth anisotropy parameter γ_λ determined from penetration depth experiments by means of μSR, is within experimental error the same as the one deduced from H_{c1} measurements. Both techniques yield a temperature-dependent γ_λ that increases with decreasing temperature from 1.6 at $T_c = 14.6$ K to 2.6 at $T = 1.6$ K. Compared to $SmFeAsO_{0.8}F_{0.2}$ and $NdFeAsO_{0.8}F_{0.2}$,[42] superconducting $FeSe_{0.5}Te_{0.5}$ is much more isotropic, but quite comparable to the "122" class of Fe-based superconductors.[63,77,81] This suggests that the direct electronic coupling of the Fe_2Se_2 layers in the 11 system is similar to the one through the intervening *Ae* layers in the "122" class of superconductors but more effective than the coupling through the *Ln*O layers in the "1111" Fe-based systems. While γ_λ increases with decreasing temperature, the anisotropy parameter of the upper critical field $\gamma_{H_{c2}}$ determined by resistivity measurements decreases.[33,38] The observed behavior is similar to that of the two-gap superconductor MgB_2 and other Fe-based superconductors and supports a two-gap scenario also in $FeSe_{0.5}Te_{0.5}$.[42] Note, however, that for MgB_2 the slopes of $\gamma_\lambda(T)$ and $\gamma_{H_{c2}}(T)$ have reversed signs[64,65] as compared to the Fe-based superconductors. The reason for this difference is still unclear. Furthermore, the value of $\lambda_{ab}^{-2}(0)$ for $FeSe_{0.5}Te_{0.5}$ extracted from μSR data as well as the values of $\lambda_{ab}^{-2}(0)$ obtained for various Fe-based superconductors fall on the Uemura plot[55] within the limits of hole-doped and electron-doped cuprates.[56] This suggests that the pairing mechanism in the Fe-based superconductors is unconventional, as is also the case for the cuprates.

Concluding, $FeSe_{0.5}Te_{0.5}$ shows evidence for two-gap superconductivity, which is reflected in the temperature dependence of λ^{-2} and by the existence of two distinct anisotropy parameters $\gamma_\lambda(T)$ and $\gamma_{H_{c2}}(T)$. The two-gap scenario is observed for most Fe-based superconductors, suggesting that this behavior is generic for layered high-temperature superconductors: it is strongly supported by various experiments for Fe-based superconductors (Ref. 80 and references therein), it is well established for MgB_2,[65,66] and there is firm evidence for two-gap superconductivity also in the cuprates.[82–85] However, it remains to be seen whether superconductivity in these classes of high-temperature superconductors has the same or a similar origin.

ACKNOWLEDGMENTS

The μSR experiments were performed at the Swiss Muon Source, Paul Scherrer Institut, Villigen, Switzerland. This work was partially supported by the Swiss National Science Foundation, the EU Project CoMePhS, the Polish Ministry of Science and Higher Education under the research project No. N N202 4132 33, and by the NCCR Program MaNEP.

*markus.bendele@physik.uzh.ch

[1] Y. Kamihara, T. Watanabe, M. Hirano, and H. Hosono, J. Am. Chem. Soc. **130**, 3296 (2008).
[2] X. H. Chen, T. Wu, G. Wu, R. H. Liu, H. Chen, and D. F. Fang, Nature (London) **453**, 761 (2008).
[3] G. F. Chen, Z. Li, D. Wu, G. Li, W. Z. Hu, J. Dong, P. Zheng, J. L. Luo, and N. L. Wang, Phys. Rev. Lett. **100**, 247002 (2008).
[4] Z.-A. Ren, J. Yang, W. Lu, W. Yi, X.-L. Shen, Z.-C. Li, G.-C. Che, X.-L. Dong, L.-L. Sun, F. Zhou, and Z.-X. Zhao, EPL **82**, 57002 (2008).
[5] Z. A. Ren, J. Yang, W. Lu, W. Yi, G. C. Che, X. L. Dong, L. L. Sun, and Z. X. Zhao, Mater. Res. Innovations **12**, 105 (2008).
[6] P. Cheng, L. Fang, H. Yang, X. Y. Zhu, G. Mu, H. Q. Luo, Z. S. Wang, and H. H. Wen, Sci. China, Ser. G **51**, 719 (2008).
[7] M. Rotter, M. Tegel, and D. Johrendt, Phys. Rev. Lett. **101**, 107006 (2008).
[8] X. C. Wang, Q. Q. Liu, Y. X. Lv, W. B. Gao, L. X. Yang, R. C. Yu, F. Y. Li, and C. Q. Jin, Solid State Commun. **148**, 538 (2008).
[9] F. C. Hsu, J. Y. Luo, K.-W. Yeh, T.-K. Chen, T.-W. Huang, P.-M. Wu, Y.-C. Lee, Y.-L. Huang, Y.-Y. Chu, D.-C. Yan, and M.-K. Wu, Proc. Natl. Acad. Sci. U.S.A. **105**, 14262 (2008).
[10] A. Subedi, L. Zhang, D. J. Singh, and M. H. Du, Phys. Rev. B **78**, 134514 (2008).
[11] H. Ogino, Y. Matsumura, Y. Katsura, K. Ushiyama, S. Horii, K. Kishio, and J. Shimoyama, Supercond. Sci. Technol. **22**, 075008 (2009).
[12] X. Zhu, F. Han, G. Mu, B. Zeng, P. Cheng, B. Shen, and H.-H. Wen, Phys. Rev. B **79**, 024516 (2009).
[13] H. Luetkens, H.-H. Klauss, M. Kraken, F. J. Litterst, T. Dellmann, R. Klingeler, C. Hess, R. Khasanov, A. Amato, C. Baines, M. Kosmala, O. J. Schumann, M. Braden, J. Hamann-Borrero, N. Leps, A. Kondrat, G. Behr, J. Werner, and B. Büchner, Nature Mater. **8**, 305 (2009).
[14] A. J. Drew, Ch. Niedermayer, P. J. Baker, F. L. Pratt, S. J. Blundell, T. Lancaster, R. H. Liu, G. Wu, X. H. Chen, I. Watanabe, V. K. Malik, A. Dubroka, M. Rössle, K. W. Kim, C. Baines, and C. Bernhard, Nature Mater. **8**, 310 (2009).
[15] Y. Mizuguchi, F. Tomioka, S. Tsuda, T. Yamaguchi, and Y. Takano, Appl. Phys. Lett. **93**, 152505 (2008).
[16] R. Khasanov, M. Bendele, A. Amato, P. Babkevich, A. T. Boothroyd, A. Cervellino, K. Conder, S. N. Gvasaliya, H. Keller, H.-H. Klauss, H. Luetkens, V. Pomjakushin, E. Pomjakushina, and B. Roessli, Phys. Rev. B **80**, 140511(R) (2009).
[17] J. Karpinski, N. D. Zhigadlo, S. Katrych, Z. Bukowski, P. Moll, S. Weyeneth, H. Keller, R. Puzniak, M. Tortello, D. Daghero, R. Gonnelli, I. Maggio-Aprile, Y. Fasano, Ø. Fischer, K. Rogacki, and B. Batlogg, Physica C **469**, 370 (2009).
[18] I. I. Mazin and J. Schmalian, Physica C **469**, 614 (2009).
[19] A. Amato, R. Khasanov, H. Luetkens, and H.-H. Klauss, Physica C **469**, 606 (2009).
[20] S. Graser, T. A. Maier, P. J. Hirschfeld, and D. J. Scalapino, New J. Phys. **11**, 025016 (2009).
[21] S. Margadonna, Y. Takabayashi, Y. Ohishi, Y. Mizuguchi, Y. Takano, T. Kagayama, T. Nakagawa, M. Takata, and K. Prassides, Phys. Rev. B **80**, 064506 (2009).
[22] B. C. Sales, A. S. Sefat, M. A. McGuire, R. Y. Jin, D. Mandrus, and Y. Mozharivskyj, Phys. Rev. B **79**, 094521 (2009).
[23] P. K. Biswas, G. Balakrishnan, D. M. Paul, C. V. Tomy, M. R. Lees, and A. D. Hillier, Phys. Rev. B **81**, 092510 (2010).
[24] P. Fischer, G. Frey, M. Koch, M. Könnecke, V. Pomjakushin, J. Schefer, R. Thut, N. Schlumpf, R. Bürge, U. Greuter, S. Bondt, and E. Berruyer, Physica B **276-278**, 146 (2000).
[25] J. Rodríguez-Carvajal, Physica B **192**, 55 (1993).
[26] S. Li, C. de la Cruz, Q. Huang, Y. Chen, J. W. Lynn, J. Hu, Y. L. Huang, F.-C. Hsu, K. W. Yeh, M. K. Wu, and P. Dai, Phys. Rev. B **79**, 054503 (2009).
[27] W. Bao, Y. Qiu, Q. Huang, M. A. Green, P. Zajdel, M. R. Fitzsimmons, M. Zhernenkov, S. Chang, Minghu Fang,B. Qian, E. K. Vehstedt, J. Yang, H. M. Pham, L. Spinu, and Z. Q. Mao, Phys. Rev. Lett. **102**, 247001 (2009).
[28] E. Pomjakushina, K. Conder, V. Pomjakushin, M. Bendele, and R. Khasanov, Phys. Rev. B **80**, 024517 (2009).
[29] T. Kamimura, J. Phys. Soc. Jpn. **43**, 1594 (1977).
[30] C. P. Bean, Phys. Rev. Lett. **8**, 250 (1962).
[31] C. P. Bean, Rev. Mod. Phys. **36**, 31 (1964).
[32] Y. Yeshurun and A. P. Malozemoff, Phys. Rev. Lett. **60**, 2202 (1988).
[33] M. H. Fang, J. H. Yang, F. F. Balakirev, Y. Kohama, J. Singleton, B. Qian, Z. Q. Mao, H. D. Wang, and H. Q. Yuan, Phys. Rev. B **81**, 020509 (2010).
[34] J. R. Clem, in Proceeding of the 13th Conference on Low Temperature Physics (LT 13), edited by K. D. Timmerhaus, W. J. O'Sullivan, and E. F. Hammel (Plenum, New York, 1974), Vol. 3, p. 102.
[35] L. Burlachkov, Phys. Rev. B **47**, 8056 (1993).
[36] L. Burlachkov, V. B. Geshkenbein, A. E. Koshelev, A. I. Larkin, and V. M. Vinokur, Phys. Rev. B **50**, 16770 (1994).
[37] M. Tinkham, *Introduction to Superconductivity* (Krieger, Malabar, Florida, 1975).
[38] H. Lei, R. Hu, E. S. Choi, J. B. Warren, and C. Petrovic, Phys. Rev. B **81**, 094518 (2010).
[39] V. G. Kogan, Phys. Rev. B **24**, 1572 (1981).
[40] V. G. Kogan, M. M. Fang, and S. Mitra, Phys. Rev. B **38**, 11958 (1988).
[41] S. Weyeneth, R. Puzniak, U. Mosele, N. D. Zhigadlo, S. Katrych, Z. Bukowski, J. Karpinski, S. Kohout, J. Roos, and H. Keller, J. Supercond. Novel Magn. **22**, 325 (2009).
[42] S. Weyeneth, R. Puzniak, N. D. Zhigadlo, S. Katrych, Z. Bukowski, J. Karpinski, and H. Keller, J. Supercond. Novel Magn. **22**, 347 (2009).
[43] L. Balicas, A. Gurevich, Y. J. Jo, J. Jaroszynski, D. C. Larbalestier, R. H. Liu, H. Chen, X. H. Chen, N. D. Zhigadlo, S. Katrych, Z. Bukowski, and J. Karpinski, arXiv:0809.4223 (unpublished).
[44] P. Zimmermann, H. Keller, S. L. Lee, I. M. Savić, M. Warden, D.

Zech, R. Cubitt, E. M. Forgan, E. Kaldis, J. Karpinski, and C. Krüger, Phys. Rev. B **52**, 541 (1995).
[45] R. Khasanov, K. Conder, E. Pomjakushina, A. Amato, C. Baines, Z. Bukowski, J. Karpinski, S. Katrych, H.-H. Klauss, H. Luetkens, A. Shengelaya, and N. D. Zhigadlo, Phys. Rev. B **78**, 220510 (2008).
[46] T. M. Riseman, J. H. Brewer, K. H. Chow, W. N. Hardy, R. F. Kiefl, S. R. Kreitzman, R. Liang, W. A. MacFarlane, P. Mendels, G. D. Morris, J. Rammer, J. W. Schneider, C. Niedermayer, and S. L. Lee, Phys. Rev. B **52**, 10569 (1995).
[47] A. Maisuradze, R. Khasanov, A. Shengelaya, and H. Keller, J. Phys.: Condens. Matter **21**, 075701 (2009).
[48] H. Schilling, M. Camani, F. N. Gygax, W. Rüegg, and A. Schenck, J. Phys. F: Met. Phys. **12**, 875 (1982).
[49] A. Yaouanc, P. Dalmas de Réotier, and E. H. Brandt, Phys. Rev. B **55**, 11107 (1997).
[50] A. Carrington and F. Manzano, Physica C **385**, 205 (2003).
[51] A. B. Vorontsov, M. G. Vavilov, and A. V. Chubukov, Phys. Rev. B **79**, 140507(R) (2009).
[52] J. Yang, M. Matsui, M. Kawa, H. Ohta, C. Michioka, C. Dong, H. Wang, H. Yuan, M. Fang, and K. Yoshimura, arXiv:0911.4758 (unpublished).
[53] T. Kato, Y. Mizuguchi, H. Nakamura, T. Machida, H. Sakata, and Y. Takano, Phys. Rev. B **80**, 180507(R) (2009).
[54] H. Kim, C. Martin, R. Gordon, M. Tanatar, J. Hu, B. Qian, Z. Mao, R. Hu, C. Petrovic, N. Salovich, R. Giannetta, and R. Prozorov, Phys. Rev. B **81**, 180503(R) (2010)..
[55] Y. J. Uemura, G. M. Luke, B. J. Sternlieb, J. H. Brewer, J. F. Carolan, W. N. Hardy, R. Kadono, J. R. Kempton, R. F. Kiefl, S. R. Kreitzman, P. Mulhern, T. M. Riseman, D. Ll, Williams, B. X. Yang, S. Uchida, H. Takagi, J. Gopalakrishnan, A. W. Sleight, M. A. Subramanian, C. L. Chien, M. Z. Cieplak, G. Xiao, V. Y. Lee, B. W. Statt, C. E. Stronach, W. J. Kossler, and X. H. Yu, Phys. Rev. Lett. **62**, 2317 (1989).
[56] A. Shengelaya, R. Khasanov, D. G. Eshchenko, D. Di Castro, I. M. Savić, M. S. Park, K. H. Kim, S.-I. Lee, K. A. Müller, and H. Keller, Phys. Rev. Lett. **94**, 127001 (2005).
[57] H. Luetkens, H.-H. Klauss, R. Khasanov, A. Amato, R. Klingeler, I. Hellmann, N. Leps, A. Kondrat, C. Hess, A. Köhler, G. Behr, J. Werner, and B. Büchner, Phys. Rev. Lett. **101**, 097009 (2008).
[58] S. Takeshita and R. Kadono, New J. Phys. **11**, 035006 (2009).
[59] J. P. Carlo, Y. J. Uemura, T. Goko, G. J. MacDougall, J. A. Rodriguez, W. Yu, G. M. Luke, P. Dai, N. Shannon, S. Miyasaka, S. Suzuki, S. Tajima, G. F. Chen, W. Z. Hu, J. L. Luo, and N. L. Wang, Phys. Rev. Lett. **102**, 087001 (2009).
[60] R. Khasanov, H. Luetkens, A. Amato, H.-H. Klauss, Z.-A. Ren, J. Yang, W. Lu, and Z.-X. Zhao, Phys. Rev. B **78**, 092506 (2008).
[61] R. Khasanov, M. Bendele, A. Amato, K. Conder, H. Keller, H.-H. Klauss, H. Luetkens, and E. Pomjakushina, Phys. Rev. Lett. **104**, 087004 (2010).
[62] F. L. Pratt, P. J. Baker, S. J. Blundell, T. Lancaster, H. J. Lewtas, P. Adamson, M. J. Pitcher, D. R. Parker, and S. J. Clarke, Phys. Rev. B **79**, 052508 (2009).
[63] R. Khasanov, D. V. Evtushinsky, A. Amato, H.-H. Klauss, H. Luetkens, Ch. Niedermayer, B. Büchner, G. L. Sun, C. T. Lin, J. T. Park, D. S. Inosov, and V. Hinkov, Phys. Rev. Lett. **102**, 187005 (2009).
[64] J. D. Fletcher, A. Carrington, O. J. Taylor, S. M. Kazakov, and J. Karpinski, Phys. Rev. Lett. **95**, 097005 (2005).
[65] M. Angst, R. Puzniak, A. Wisniewski, J. Jun, S. M. Kazakov, J. Karpinski, J. Roos, and H. Keller, Phys. Rev. Lett. **88**, 167004 (2002).
[66] M. Angst and R. Puzniak, in *Focus on Superconductivity*, edited by B. P. Martines (Nova Science, New York, 2004), Vol. 1, pp. 1–49.
[67] R. S. Gonnelli, D. Daghero, M. Tortello, G. A. Ummarino, V. A. Stepanov, R. K. Kremer, J. S. Kim, N. D. Zhigadlo, and J. Karpinski, Physica C **469**, 512 (2009).
[68] P. Samuely, Z. Pribulová, P. Szabó, G. Pristáš, S. L. Bud'ko, and P. C. Canfield, Physica C **469**, 507 (2009).
[69] P. Szabó, Z. Pribulová, G. Pristáš, S. L. Bud'ko, P. C. Canfield, and P. Samuely, Phys. Rev. B **79**, 012503 (2009).
[70] G. Li, W. Z. Hu, J. Dong, Z. Li, P. Zheng, G. F. Chen, J. L. Luo, and N. L. Wang, Phys. Rev. Lett. **101**, 107004 (2008).
[71] G. Mu, H. Luo, Z. Wang, L. Shan, C. Ren, and H. H. Wen, Phys. Rev. B **79**, 174501 (2009).
[72] C. Ren, Z. S. Wang, H. Q. Luo, H. Yang, L. Shan, and H. H. Wen, Phys. Rev. Lett. **101**, 257006 (2008).
[73] F. Hunte, J. Jaroszynski, A. Gurevich, D. C. Larbalestier, R. Jin, A. S. Sefat, M. A. McGuire, B. C. Sales, D. K. Christen, and D. Mandrus, Nature (London) **453**, 903 (2008).
[74] S. Weyeneth, M. Bendele, R. Puzniak, F. Muranyi, A. Bussmann-Holder, N. D. Zhigadlo, S. Katrych, Z. Bukowski, J. Karpinski, A. Shengelaya, R. Khasanov, and H. Keller, arXiv:0911.5420 (unpublished).
[75] L. Malone, J. D. Fletcher, A. Serafin, A. Carrington, N. D. Zhigadlo, Z. Bukowski, S. Katrych, and J. Karpinski, Phys. Rev. B **79**, 140501(R) (2009).
[76] M. Hiraishi, R. Kadono, S. Takeshita, M. Miyazaki, A. Koda, H. Okabe, and J. Akimitsu, J. Phys. Soc. Jpn. **78**, 023710 (2009).
[77] R. Khasanov, A. Maisuradze, H. Maeter, A. Kwadrin, H. Luetkens, A. Amato, W. Schnelle, H. Rosner, A. Leithe-Jasper, and H.-H. Klauss, Phys. Rev. Lett. **103**, 067010 (2009).
[78] J. Nagamatsu, N. Nakagawa, T. Muranaka, Y. Zenitani, and J. Akimitsu, Nature (London) **410**, 63 (2001).
[79] R. S. Gonnelli, D. Daghero, G. A. Ummarino, V. A. Stepanov, J. Jun, S. M. Kazakov, and J. Karpinski, Phys. Rev. Lett. **89**, 247004 (2002).
[80] D. V. Evtushinsky, D. S. Inosov, V. B. Zabolotnyy, M. S. Viazovska, R. Khasanov, A. Amato, H.-H. Klauss, H. Luetkens, Ch. Niedermayer, G. L. Sun, V. Hinkov, C. T. Lin, A. Varykhalov, A. Koitzsch, M. Knupfer, B. Büchner, A. A. Kordyuk, and S. V. Borisenko, New J. Phys. **11**, 055069 (2009).
[81] Z. Bukowski, S. Weyeneth, R. Puzniak, P. Moll, S. Katrych, N. D. Zhigadlo, J. Karpinski, H. Keller, and B. Batlogg, Phys. Rev. B **79**, 104521 (2009).
[82] R. Khasanov, A. Shengelaya, A. Maisuradze, F. La Mattina, A. Bussmann-Holder, H. Keller, and K. A. Müller, Phys. Rev. Lett. **98**, 057007 (2007).
[83] A. Bussmann-Holder, R. Khasanov, A. Shengelaya, A. Maisuradze, F. La Mattina, H. Keller, and K. A. Müller, EPL **77**, 27002 (2007).
[84] R. Khasanov, A. Shengelaya, J. Karpinski, A. Bussmann-Holder, H. Keller, and K. A. Müller, J. Supercond. Novel Magn. **21**, 81 (2008).
[85] R. Khasanov, S. Strässle, D. Di Castro, T. Masui, S. Miyasaka, S. Tajima, A. Bussmann-Holder, and H. Keller, Phys. Rev. Lett. **99**, 237601 (2007).